JOURNAL OF SPACECRAFT AND ROCKETS
Vol. 29, No. 5, September-October 1992

Effect of Aluminized-Grain Design on Slag Accumulation

E. Hess,* K. Chen,* P. Acosta,* D. Brent,† and F. Fendell‡
TRW Space and Technology Group, Redondo Beach, California 90278

A parametric investigation was carried out, by analytic and numeric solution of a simple Eulerian-potential-flow/Lagrangian-particle-tracking formulation, of the effect of metallized-grain configuration on the retention of slag within the cavity of a first-stage-type solid-rocket-propellant motor. In particular, a relatively short motor with the grain deeply slotted near the aft end, a relatively long motor also with the grain deeply slotted near the aft end, and a long "conocyl" motor with axially distributed slots (such that much of the aft end was grain filled during the entire burn) were compared. The same initial grain bore and the same casing diameter pertained to all three motors, and in each case the nozzle was taken to be deeply recessed ("submerged"). It was found that, over a wide range of plausible particle sizes, the accumulation of slag (here, molten aluminum oxide) at the aft end is appreciably less for the short motor and for the conocyl motor than for the long motor. Further, it was found that the effect of a plausible flight-acceleration history on slag retention, relative to a standard-gravity calculation, would be discernible only for larger particle sizes, above roughly 200-μm diameter.

Nomenclature

d_i = effective diameter of alumina particles in size category i, m
$F(t)$ = dimensionless time-varying function defining the recirculation-flow boundary
g = magnitude of the acceleration of gravity, m/s^2
M_{Al} = mass of aluminum retained in the motor cavity, kg
$M_{Al_2O_3}$ = mass of alumina retained in the motor cavity, kg
p_0 = (uniform) motor-cavity pressure, Pa
$\dot{R}_s$ = nominal grain-regression rate, m/s
$\dot{R}_s^*$ = enhanced grain-regression rate for the star-slotted grain, m/s
R_0 = radius at ignition of the slot-free nose-end bore, m
R_1 = radius of the bore of the slotted section of the conocyl grain, m
R_2 = inner radius of the motor casing, m
R_3 = radius at the entrance to the submerged nozzle, m
$R_s^{(i)}(t)$ = radius at time t of slot i of the conocyl motor, m
T_0 = (uniform) motor-cavity temperature, K
t = time, with ignition at $t = 0$, s
t_b = time at which the grain burning is completed, s
t_s = value of time used to define the recirculation-flow boundary, s
V_{di} = volume of the grain whose aluminum content is retained as alumina, m^3
W_j = molecular weight of species j, kg/mole
X_{Al} = volume fraction occupied by aluminum
x = axial coordinate, measured from the nose end of the grain, m
$x_d^{(i)}(t)$ = axial position at time t of the downwind boundary of slot i of the conocyl motor, m
$x_u^{(i)}(t)$ = axial position at time t of the upwind boundary of slot i of the conocyl motor, m
$x_1(t)$ = length of the slot-free grain at the nose end, m
$x_2(t)$ = position of the aft end of the grain at time t, m
x_3 = axial position of the recessed-nozzle entrance, m
x_4 = length from the nose of the grain to the base of the casing (excluding the nozzle), m
Y_{Al} = mass fraction of aluminum
κ = factor defining the recirculation-flow boundary
ν_j = stoichiometric coefficient of species j in the aluminum-oxygen reaction, moles
ρ_{Al} = density of aluminum, kg/m^3
ρ_g = (uniform) gas density in the motor cavity, kg/m^3
ρ_s = density of alumina, kg/m^3
ρ_{sg} = density of the grain, kg/m^3
ρ_1 = density of that portion of the grain that becomes gas after combustion, kg/m^3
ρ_2 = density of that portion of the grain that becomes alumina after combustion, kg/m^3
ϕ_{di} = fraction of the aluminum mass that evolves from the grain as alumina particles of diameter d_i

Introduction

THE combustion of a typical metallized composite solid propellant grain,[1] consisting of relatively small aluminum particles (~ 20% by mass, 3–30 μm in size) and relatively large ammonium-perchlorate crystals (~ 65% by mass, 40–300 μm in size) dispersed in a synthetic-rubber matrix (~ 15% by mass), results in the formation of molten aluminum-oxide (alumina) particles, which range in size from approximately one to several hundred microns. Though exceptions exist, in general, the small particles (less than 10 μm) exhibit no appreciable velocity slip with respect to the combustion-product-gas motion in the subsonic flow of the motor chamber; however, larger particles exhibit finite velocity slip[2] with respect to the instantaneously collocated gas and may be retained in a slag pool near the aft end of the motor chamber during flight. The accumulation of slag creates concerns about motor case heating, reduces the motor impulse, adds inert weight to the motor, may interfere with the thrust vector control mechanism, and may result in undesirable sloshing behavior (with intermittent asymmetric expulsion of slugs of slag through the nozzle).

A theoretical study was undertaken to characterize the slag retention for several axisymmetric slotted grain configurations. The number, size, and locations of slots were varied for a given motor casing; the length (but not the radial dimensions) of the casing—and hence of the grain—was also varied. Furthermore, the effect of flight-acceleration history on slag retention was also examined. However, with few exceptions, the composition of the grain was held fixed at a nominal, typical makeup. To the extent that an equivalent-bore-area

Received Dec. 16, 1991; revision received March 3, 1992; accepted for publication March 3, 1992.

*Member of the Technical Staff, Center for Propulsion Technology and Fluid Mechanics.
†Section Head, Center for Propulsion Technology and Fluid Mechanics. Member AIAA.
‡Staff Engineer, Center for Propulsion Technology and Fluid Mechanics. Associate Fellow AIAA.

axisymmetric model can describe the dilutely-particle-laden two-phase flow in an azimuthally periodic (i.e., "star-slotted") grain,[3] slag retention in more general, three-dimensional grain configurations may be undertaken by the analysis described in this paper. The enhanced mass transfer associated with a star-slotted grain may be simulated by 1) attributing an enhanced perimeter (with the nominal burn rate) for the equivalent-bore area; or, as adopted here, 2) attributing an enhanced burn rate (with the nominal perimeter) for the equivalent-bore area.

Procedure

In the absence of precise measurements of the particle-size distribution, and even of the total slag retention in the combustion chamber at the completion of a burn, only simple modeling of the two-phase flow in the first-stage-type motors of interest here (basically radially burning, with large length-to-diameter ratio) seems worth undertaking. Thus, we perform a two-step sequence of calculations,[4,5] in which classical potential-flow theory is adopted to obtain the gas-phase flow in Eulerian form, and then Lagrangian particle tracking is carried out in that flow (with a suitably generalized Stokes drag and with vehicle/gravitational acceleration), to obtain the slag-particle trajectories. It is taken that 1) the flow within the chamber is highly subsonic and thermodynamically uniform (and known), to good approximation; 2) the rate of grain recession is constant (and known); 3) the flowfield is quasi-steady; and 4) the grain configuration (readily evolved for any later time during the burn from a specified initial configuration) during the flight of any one particle is effectively invariant. Thus, the flowfield and the particle paths both are obtained at each of several distinct times during the burn, for each of several particle sizes. The adoption of a quasisteady inviscid model for a duct-type flow with large mass "injection" seems not unreasonable.

Gas-Phase Flowfield

Two mathematical treatments of the same physical formulation were undertaken. The (cylindrical) radial and axial velocity components of the potential flow are obtained more meticulously, but more tediously, by use of a finite element solution of Laplace's equation subject to Neumann boundary conditions, after a computational mesh is established for the highly convoluted gas/grain-boundary geometry. The gas-phase flowfield is obtained more rapidly, but less precisely, by applying[4] the continuity equation, first in the "large" (integral) form to obtain the axial velocity component, then in the "small" (differential) form to obtain the radial velocity component, under the conjecture that a generalized counterflow well represents the motion.[6]

Lagrangian Particle Tracking

The alumina particles are taken to be spherical and to be formed instantaneously at the gas-grain interface. The complication of a rate equation would have to be added to permit a finite-rate conversion of the aluminum to oxide during flight; the details would be conjectural, and probably most of the oxidation occurs very close to the gas-grain interface. The just-formed particles at the interface are accelerated from a state of rest relative to the grain. They are subject to fluid (Stokes, transitional, and turbulent drag in accord with the magnitude of the local Reynolds number, based on the magnitude of the local velocity difference between the gas and the particles), inertial and gravitational forces, and forces associated with vehicle-acceleration. Under the inviscid-flowfield model, there is a finite slip velocity for the gas flow, so the alumina particles leave their site of formation with a finite velocity tangential to the gas-grain interface, as well as a finite velocity normal to the interface. The finite velocity components of the particles at the gas-grain interface are computed by previously described procedures.[4] Collisional effects, anticipated (for the fairly moderate particle loading of interest) to be of consequence for particles near the axis of symmetry only, are omitted, since near-axis particles are taken to enter the nozzle and thus not to contribute to slag accumulation. If the trajectory of a particle crosses the plane of the deeply recessed nozzle entrance without entering the nozzle, or if the molten particle otherwise makes contact with any in-cavity surface during its transit toward the nozzle, that particle is regarded as retained within the cavity.

The trajectories of a sufficient number of particles (of each "size range") are computed at each of a sufficient sequence of times during the burn. By "sufficient" it is meant that it is possible to estimate what portion of the aluminum, taken initially to be homogeneously distributed throughout the grain, is retained somewhere within the motor cavity in the form of alumina. More precisely, the time evolution of a geometric surface ("separatrix") is calculated that distinguishes the portion of the grain aluminum that [on being transformed to an alumina particle of a given size at the (advancing) gas-grain boundary] exits the chamber, from the portion of grain aluminum that does not. The total mass of (oxidated) aluminum that is retained requires the adoption, on whatever basis, of an alumina particle-size distribution. For simplicity, we plausibly take the particle-size distribution not to change during the burn since we take the thermodynamic state and regression rate not to change significantly during most of the burn. (In fact, after ignition and flame filling, the pressure may rise modestly above the nominal burn pressure, then decrease moderately below that pressure near burn completion.)

Of course, the advantage of such a simplistic model is that parametric variations may be pursued relatively quickly and easily and thus relatively thoroughly. Slag-retention estimations by this type of model were presented recently by Haloulakos[7] for an end-burning upper-stage motor, and the present results for a laterally burning, first- or second-stage motor serve to complement his work.

Results

Parameter Assignments

Internal flowfields and particle trajectories were calculated on Compaq 386/25 and Zenith 386/16 desktop computers, for both vertical static and plausible flight conditions, typically at the times 0+ (ignition), 5, 10, 15, 20, 25, 30, 35, and 40 s (approximately the duration of the burn); characteristically, trajectories were predicted at each of these times during the burn for particles with at least the following particle diameters: 25, 50, 75, 100, 200, 300, 400, and 500 μm. The calculations in general were carried out (with close agreement) by both the approximate counterflow-based treatment and the finite element based treatment of the two-phase flow, for the purpose of adding credibility to the findings; the computer codes themselves were checked against known closed-form solutions available for simple geometries. For a given motor at a given time during the burn, for a given size of particle, about 50 particle trajectories could be computed with the counterflow velocity field in less than 1 m of computer time; obtaining the flowfield by finite element solution and then using it to compute the trajectories required about 10 m of computer time.

The three hypothetical grain configurations to be examined (Figs. 1–4) all have basically the same inner bore at ignition, the same outer diameter, and the same deeply submerged nozzle. The three grain configurations differ as follows: the relatively short motor has deeply cut slots at the aft end; the long motor has about 23% more grain but also has deeply cut slots at the aft end; and the conocyl motor has the same length as the long motor, also has slots (so that the mass throughput is fairly constant during the burn), but has its slots so axially distributed that the aft end remains relatively grain filled during the burn.

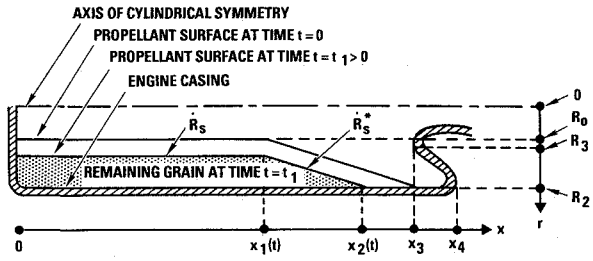

Fig. 1 Sketch of the long or short motor (not to scale), with the grain geometry and the re-entrant nozzle depicted. Over the axial span $x_2(t) > x > x_1(t)$, the grain is star shaped; in the equivalent-bore axisymmetric model, an enhanced grain-regression rate $\dot{R}_s^*$ is adopted. For $x_1(t) \geq x \geq 0$, a cylindrical bore exists and regression rate $\dot{R}_s (< \dot{R}_s^*)$ holds.

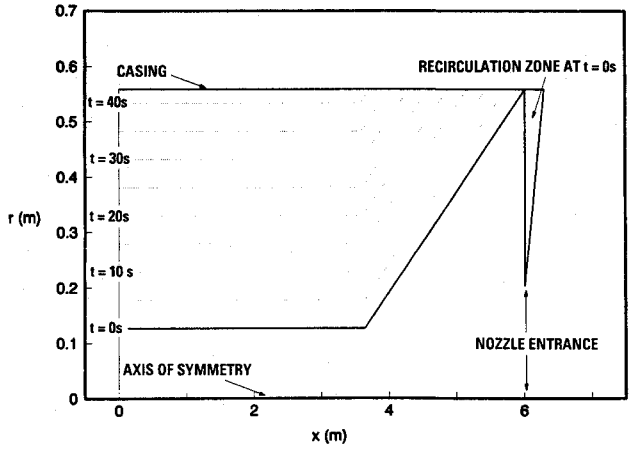

Fig. 2 Grain configuration for a sequence of times during the burn, for the long motor, with ignition at time $t = 0$. The recirculation zone is depicted for $t = 0$ only and extends from the nozzle-entrance perimeter (R_3, x_3) to the grain tip $[R_2, x_2(0)]$.

The following baseline parameter assignments hold for all reported results unless explicit statement is made to the contrary ($t = 0$ is recalled to be time of ignition):

$$\begin{aligned} p_0 &= 10.1 \text{ MPa} & T_0 &= 3650 \text{ K} \\ \rho &= \rho_g = 9.29 \text{ kg/m}^3 & \rho_1 &= 1295 \text{ kg/m}^3 \\ \rho_s &= 3965 \text{ kg/m}^3 & \rho_{sg} &= 1850 \text{ kg/m}^3 \\ \dot{R}_s &= 1.016 \times 10^{-2} \text{ m/s} & \dot{R}_s^* &= 1.030 \times 10^{-2} \text{ m/s} \\ x_4 &= 6.3 \text{ m} & R_0 &= 0.13 \text{ m} \\ R_2 &= 0.56 \text{ m} & R_3 &= 0.20 \text{ m} \end{aligned} \tag{1}$$

where p_0 and T_0 are the (uniform) pressure and temperature, respectively, in the combustion chamber; ρ_g is the (uniform) gas density in the combustion chamber; ρ_1 is the mass of propellant that turns into gas per unit volume of propellant; ρ_{sg} is the (total) mass of propellant per unit volume of propellant; ρ_s is the mass of alumina per unit volume occupied by alumina (the value adopted holds for ambient conditions—smaller values may hold under rocket-chamber conditions); $\dot{R}_s$ is the nominal grain-regression rate; $\dot{R}_s^*$ is the enhanced grain-regression rate pertinent for modeling of star-slotted portions of the grain (if any); x_4 is the longest definable length of the rocket from the nose of the grain to the base of the casing (excluding the nozzle); R_0 is the radius, at time $t = 0$, of the long slot-free portion of the bore near the nose end, $0 \leq x \leq x_1(t)$, where x is the axial coordinate and $x = 0$ is the nose end of the grain; R_2 is the (inner) radius of the motor casing; and R_3 is the radius at the entrance to the deeply submerged nozzle. More explicitly, R_3 is the nozzle radius at axial station x_3, the plane (perpendicular to the axis of symmetry) that is just tangent to the nozzle entrance. The quantity x_4 plays only a small role in the analysis. The mass fraction of aluminum in the grain for these parameter assignments is about 0.16.

For the long motor,

$$x_1(0) = 3.6 \text{ m}, \quad x_2(0) = 6.0 \text{ m}, \quad x_3 = 6.02 \text{ m} \tag{2}$$

For the short motor,

$$x_1(0) = 2.0 \text{ m}, \quad x_2(0) = 4.3 \text{ m}, \quad x_3 = 4.3 \text{ m}, \quad x_4 = 4.6 \text{ m} \tag{3}$$

The quantity $x_1(0)$ is the axial position (i.e., length) at ignition of the slot-free portion of the grain at the nose end. An axisymmetric model is adopted for the star-slotted domain $x_1(0) < x < x_2(0)$, where $x_2(0)$ is the axial position at ignition marking the most downwind position at which any grain exists. The quantity x_3 has already been defined to be the axial plane containing the mouth of the deeply recessed nozzle. In general, $x_4 > x_3 > x_2 > x_1 > 0$ at any time. Also, the grain is so configured that the last-to-burn portion of the grain at any axial site lies contiguous to the motor casing. Figures 2 and 3 present the grain configuration for several times during the burn for the long motor and the short motor, respectively. The calculation of $x_1(t)$ and $x_2(t)$ has been discussed previously (see the Appendix in Ref. 4).

For the conocyl motor, the parameter values assigned in Eqs. (1) and (2) still hold, except that

$$R_0 = 0.11 \text{ m}, \quad x_1(0) = 4.7 \text{ m}, \quad x_2(0) > x_3 \tag{4a}$$

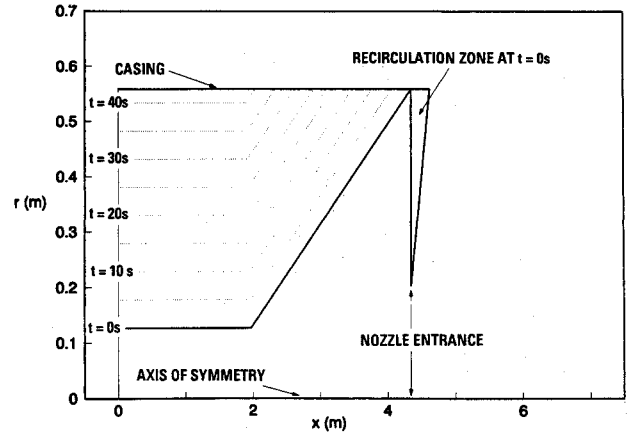

Fig. 3 Same as Fig. 2, but for the short motor.

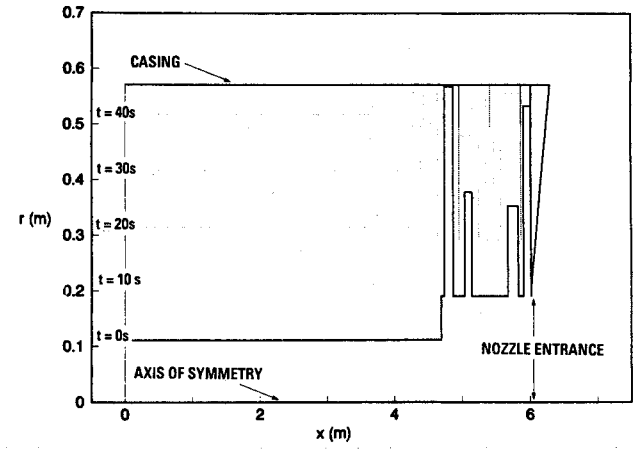

Fig. 4 Same as Fig. 2, but for the conocyl motor. There is no early time recirculation zone because the aft end of the chamber is grain-filled. Four axisymmetric slots are cut into the larger bore toward the aft end, so all grain surfaces regress at the rate $\dot{R}_s$.

in the sense that grain extends well beyond the nozzle entrance plane. The conocyl motor has a bore, initially of radius R_0 and without slots, in $0 \le x \le x_1(0)$. It also has a bore, initially of radius R_1 and with four slots, in $x_1(0) < x < x_3$; the four slots, each of right-circular-cylinderlike configurations, are cut (in general) with different "mouth openings" and to different depths into the grain. The mouth openings lie between $x_u^{(i)}(t) < x < x_d^{(i)}(t)$, and extend to a radius $R_s^{(i)}(t)$ from the axis of symmetry, $i = 1, 2, 3, 4$. We adopt

$$x_u^{(1)}(0) = 4.74 \text{ m}, \quad x_d^{(1)}(0) = 4.87 \text{ m}, \quad R_s^{(1)}(0) = 0.57 \text{ m}$$

$$x_u^{(2)}(0) = 5.04 \text{ m}, \quad x_d^{(2)}(0) = 5.14 \text{ m}, \quad R_s^{(2)}(0) = 0.38 \text{ m}$$

$$x_u^{(3)}(0) = 5.68 \text{ m}, \quad x_d^{(3)}(0) = 5.83 \text{ m}, \quad R_s^{(3)}(0) = 0.35 \text{ m} \quad (4b)$$

$$x_u^{(4)}(0) = 5.90 \text{ m}, \quad x_d^{(4)}(0) = 6.02 \text{ m}, \quad R_s^{(4)}(0) = 0.53 \text{ m}$$

$$R_1 = 0.19 \text{ m}$$

The mouth openings of the cylindrical slots are of sufficient thickness that the slots are not inadvertent sonic nozzle inlets for anomalous, radially outward flow of bore fluid, especially during early stages of the burn, so this aspect of the design seems free of local pressure-rise difficulties. On the other hand, the idealized, sharp corners on the slots would be rounded in practice; otherwise, forces on the grain result in a slump of the grain into the bore, with possibly catastrophic pressure-rise consequences. Figure 4 presents the grain configuration for several times during the burn for the conocyl motor. The slots can, and do, merge in time. The regression rate $\dot{R}_s$ pertains to the cylindrically symmetric grain in $0 < x < x_1(t)$, and $\dot{R}_s^*$ pertains to the cylindrically symmetric model of a star-slotted grain in $x_1(t) < x < x_2(t)$, for the long and short motors; however, for the conocyl motor, axisymmetry holds for the entire grain, bores, and slots, so that $\dot{R}_s$ is used to compute the regression of all gas-grain interfaces. For the counterflow model, no flowfield or particle-tracking analysis is undertaken within any slot at any time for the conocyl motor; details of the in-slot flow do not appear to be essential for present purposes. The computed gaseous efflux from any slot is distributed uniformly across the mouth of that slot in calculating the gas-phase velocity components, and alumina particles are tracked from the mouth of the slot. If a separatrix, at any given time for any given particle size, lies at the mouth of a slot, the separatrix is assigned any axial position (between the upwind and downwind ends of the slot, at the

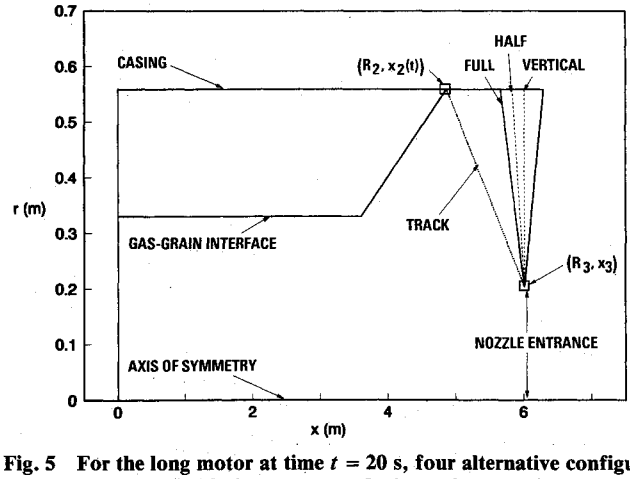

Fig. 5 For the long motor at time $t = 20$ s, four alternative configurations for the recirculation zone are depicted. The defining stream surface of the largest recirculation zone tracks the downwind end of the grain $x_2(t)$, as it moves upwind; the defining stream surface of the next largest recirculation zone tracks $x_2(t)$, but only until $[x_3 - x_2(t)] = (R_2 - R_3)$ (full exit plane annulus), then stops; of the next largest, until $[x_3 - x_2(t)] = 0.5(R_2 - R_3)$ (half exit plane annulus), then stops; and of the smallest, until $[x_3 - x_2(t)] = \epsilon(R_2 - R_3)$, $\epsilon \to 0$.

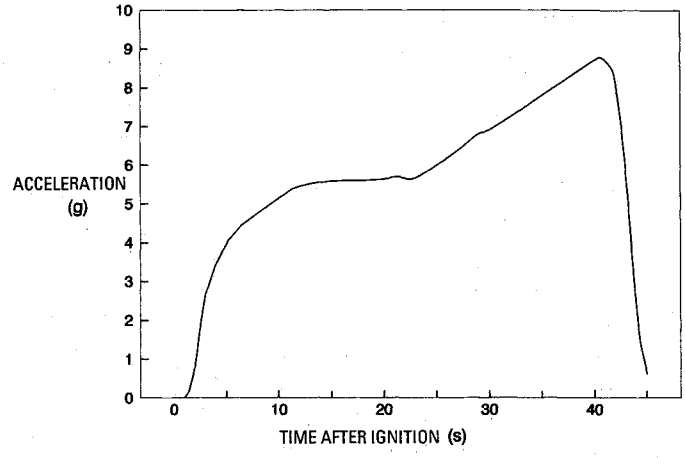

Fig. 6 Magnitude of the axial flight-acceleration history adopted for the particle-trajectory calculations. [For comparative, static test calculations, the axial acceleration is taken to be constant at the value of normal gravity (denoted 1 g).]

mouth of the slot) that leads to a smooth description of the separatrix in time.

Although the very aft end of the chamber remains largely grain filled throughout most of the burn for the conocyl motor, grain-free volumes exist at the aft end of the long and short motors, and portions of these volumes are taken to be the site of slowly recirculatory flow.[8] Within the recirculation zones, the gas-phase velocity is reasonably approximated to be zero. Any particle that crosses the stream surface that marks the interface between the recirculatory gas and the gas entering the nozzle mouth cannot leave the recirculation zone and is retained in the cavity; the only motivation for continuing to track the trajectory of such a particle after it enters the recirculation zone is to ascertain its ultimate point of impact (if any) on the casing.[9] (Particle impact on the nozzle[10,11] is outside the scope of the present investigation.) Incidentally, with a quasi-steady inviscid model, the recirculatory flow was "always there" in the sense that any vortical, recirculatory region is the consequence of unspecified, earlier, transient phenomena;[12] all of the gas evolved from the grain enters the nozzle and none enters the recirculation zone. The stream surface that defines the spatial extent of any recirculatory-flow domain[8] is specified as an input, in accord with the following adopted conventions. Any grain-free volume downwind of x_3 has recirculatory flow, but no region upwind of $x_2(t)$ has recirculatory flow. For $x_3 > x > x_2(t)$, recirculatory flow exists at all radial positions between a conical stream surface and the motor casing (Fig. 5). The conical surface is the lateral face of the frustum of a cone. Conceptually, the smaller downwind base plane of the frustum is defined by the circle $r = R_3$ at $x = x_3$, where r is the cylindrical radial coordinate (Fig. 1); we recall that R_3 is the radius of the nozzle at x_3, the axial position of the entrance to the nozzle. The larger, upwind base plane of the frustum is defined by the circle $r = R_2$, the (inner) radius of the motor casing; the axial position of the larger base plane is given by $\{x_3 - [x_3 - x_2(t)]f(t)\}$, where the given function $f(t)$ obeys the inequality $1 \ge f(t) \ge 0$. If $f(t) = 1$, the recirculation zone is said to track the downwind end of the remaining grain; if $f(t) \to 0$, there is virtually no recirculation zone upwind of the nozzle entrance plane. Often we assign $f(t) = 1$ for $0 \le t \le t_s$, where t_s ($< t_b$, the time of grain burn out) is defined by $|x_3 - x_2(t)| = \kappa(R_2 - R_3)$, where the given factor κ obeys the inequality $0.5 \le \kappa \le 1$, and $x_2(0) \simeq x_3$; for $t_b \ge t \ge t_s$, $f(t) = f(t_s)$, so that the axial site of the larger base plane is fixed over this time interval. For $\kappa = 0.5$, we refer in the following to a "half" (exit-plane-annulus) recirculatory zone; for $\kappa = 1$, we refer to a "full" (exit-plane-annulus) recirculatory zone. Clearly this parameterization is a consequence of the dearth of experimental data on in-cavity behavior under hot-flow conditions.

All particle-trajectory calculations involve an axial body force, taken to be either the constant force associated with gravity (termed henceforth the "static" case and implying a test firing in vertical orientation) or a time-varying force (Fig. 6) simulating the effect of in-flight acceleration (termed henceforth the "flight" case).

Findings

Figures 7, 8, and 9 present particle paths, computed at time $t = 20$ s into the burn under normal gravity of the long motor depicted in Fig. 2, for particles of diameter 20, 150, and 500 μm, respectively. The smaller alumina particles delineate paths that are virtually identical with stream surfaces; but some of the larger particles undergo slip relative to the flow, enter the recirculation zone, and fail to enter the nozzle. In general, the retained particles are generated from grain-gas interface toward the aft end of the motor toward the end of the burn. In Figs. 7, 8, and 9, the recirculation zone is chosen to extend from the nozzle entrance plane to the downwind extremity of the grain [$f(t) = 1$]. Figure 10 presents the particle paths computed at time $t = 20$ s into the burn under normal gravity of the conocyl motor depicted in Fig. 4, for particles of diameter 50 μm. The axial position of the separatrix distinguishes the position on the gas-grain interface downwind from which all of the emerging particle trajectories ultimately fail to enter the nozzle mouth, but upwind from which all of the particle trajectories ultimately do enter the nozzle mouth. It is very

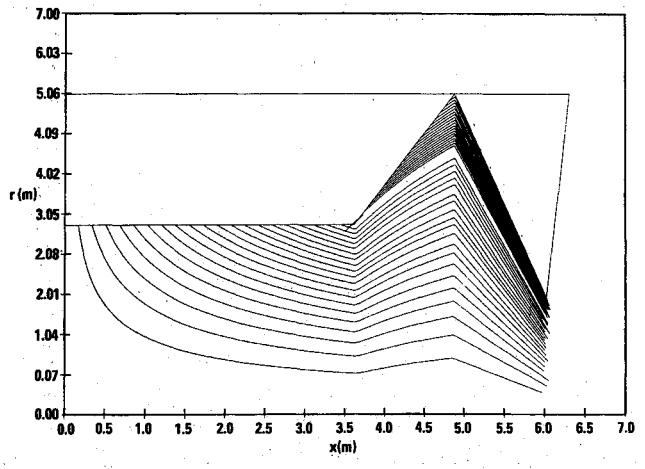

Fig. 7 Trajectories of alumina particles of 20-μm diam emerging from the gas-grain interface at time $t = 20$ s into the burn of the long motor, for a grain-tracking recirculation zone [$f(t) = 1$]. Here $Y_{Al} = 0.18$ and $\rho_{sg} = 1850$ kg/m^3 (off-nominal conditions).

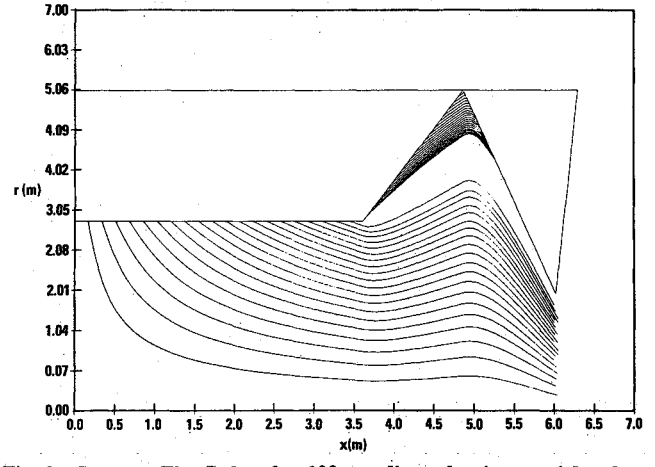

Fig. 8 Same as Fig. 7, but for 100-μm-diam alumina particles that slip more readily with respect to the gas flow, so some particles are retained in the cavity.

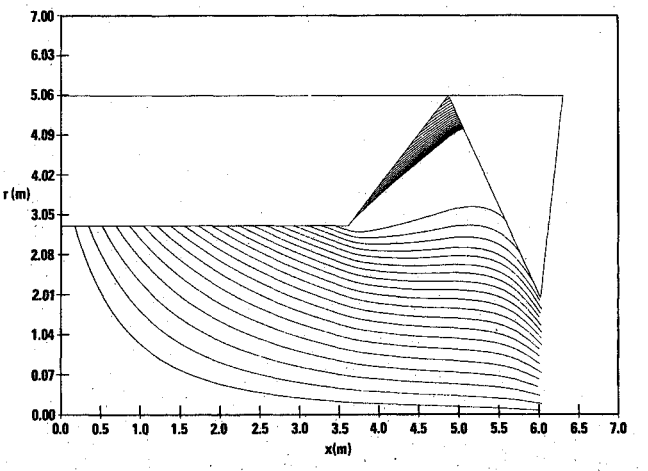

Fig. 9 Same as Fig. 7, but for 500-μm-diam particles that tend to follow trajectories quite distinct from the stream surfaces and are retained in greater numbers.

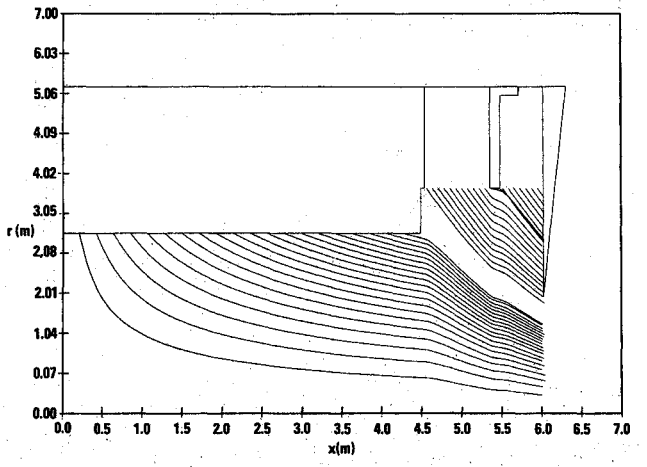

Fig. 10 Same as Fig. 7, but for 20-μm-diam alumina particles, emerging at time $t = 20$ s into the burn of the conocyl motor. No particle tracking within slots is undertaken.

tedious, but straightforward, to evolve an Eulerian particle-density field from the Lagrangian calculation; however, computing such a particle-density field is not an objective here.

Figure 11 presents the trace over the duration of the burn of the position of the separatrix holding for each of four distinct alumina-particle diameters. Figure 11 holds for the long motor under static firing (Fig. 6) for a recirculation zone characterized by $\kappa = 1$. The analogous traces (over time) of the separatrices holding for each of the same four distinct alumina particle diameters for the conocyl motor under static firing is given by Fig. 12.

The mass M_{Al} of aluminum retained in the motor cavity in the form of alumina particles of a given size d_i is given by

$$M_{Al,d_i} = \rho_{Al}\phi_{d_i}V_{d_i}X_{Al} \tag{5}$$

where ρ_{Al} is the (known) density of aluminum (mass of aluminum per volume occupied by aluminum); V_{d_i} is the volume of the grain whose aluminum content is retained as alumina (as determined by numerical integration, using the separatrix curve for particles of diameter d_i); X_{Al} is the volume of aluminum per volume of grain; and ϕ_{d_i} is the (given) fraction of the aluminum mass that evolves from the grain as alumina particles of diameter d_i. The quantity M_{Al} may be computed, since

$$X_{Al} = \frac{Y_{Al}}{(\rho_{Al}/\rho_{sg})} \tag{6}$$

where again Y_{Al} is the (given) mass fraction of the aluminum in the grain and ρ_{sg} is the (given) density of the grain (mass of

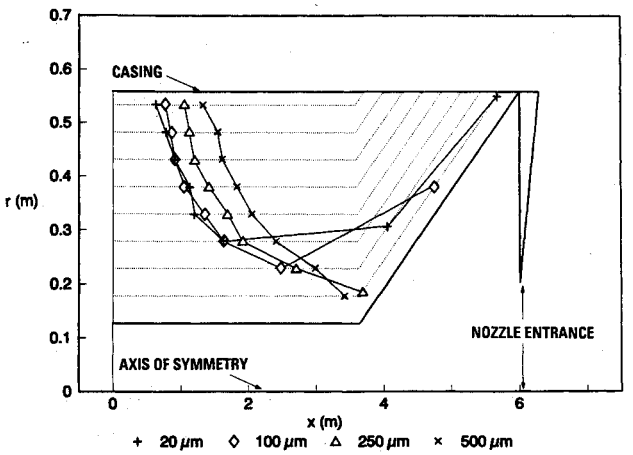

Fig. 11 Loci in time of separatrices for four particle-diameter sizes, for the long motor with a full-exit-plane annulus recirculation zone (see Fig. 5 and the penultimate paragraph under Results—Parameter Assignments) under static firing. Separatrices distinguish the nose-end gas-grain interface sites, which spawn particles that enter the nozzle mouth, from the aft-end sites that spawn retained particles. Here, $Y_{Al} = 0.18$ and $\rho_{sg} = 1850$ kg/m^3 (off-nominal conditions).

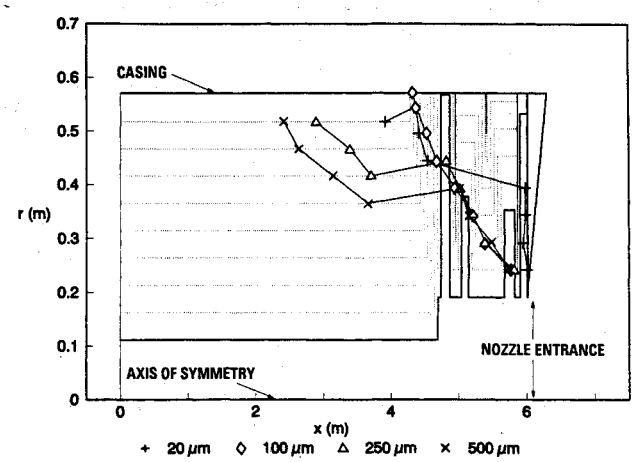

Fig. 12 Same as Fig. 11, but for the conocyl motor (so recirculation-zone considerations do not enter).

grain per volume occupied by the grain). The mass of alumina retained in the form of alumina particles of diameter d_i is given by

$$M_{Al_2O_3,d_i} = M_{Al,d_i}\left(\frac{\nu_{Al_2O_3} W_{Al_2O_3}}{\nu_{Al} W_{Al}}\right) \tag{7}$$

where ν_j is the stoichiometric coefficient of species j, and W_j is the molecular weight of species j. Since

$$4\ Al + 3\ O_2 \rightarrow 2\ Al_2O_3 \tag{8}$$

then the factor in parentheses in Eq. (7) is about 1.89. By summing over i (i.e., over the number of discrete alumina-particle sizes taken to be present), one can estimate the total slag retained according to the present model. We here shall not adopt discrete-particle-size distributions because we believe the empirical guidance available from full-scale motor burns is too meager; rather, we shall content ourselves with presenting the total slag retained were all of the aluminum to be converted to alumina particles of size d_1 (or d_2 or d_3 . . .). The results can then be used to obtain the slag accumulation for any alumina particle size distribution of interest.

Figure 13 presents the slag retention for the short motor, for both static testing and under flight acceleration; several recirculation-zone scenarios are included for the short motor. Figure 14 presents the slag retention for the long motor and for the conocyl motor, for both static testing and under flight acceleration, again with several recirculation-zone scenarios. We find that, for smaller particles, slag accumulation is moderately greater for a smaller recirculation-zone, for which the direction of the aft-end flow undergoes more abrupt change and is relatively insensitive to the applied accelerations under discussion. For larger particles, slag accumulation is appreciably greater under flight (as opposed to static) conditions and is not sensitive to the recirculation-zone models under discussion. The transition from smaller-particle to larger-particle behavior occurs roughly over the 100–300 μm particle-diameter range. Under static firing, and hence relatively modest axial acceleration, smaller particles may follow the flow into effectively crevicelike regions (whereas larger particles may not); the smaller particles then may not be able to follow the streamlines out of the crevicelike region. Thus, smaller particles may be retained under conditions for which large particles tend to enter the nozzle mouth. Larger axial acceleration acts to negate the turning toward the axis of large particles and to increase the in-cavity retention of such particles. The nonmonotonicity of slag retention with particle size for some parameter combinations seems noteworthy. Also, if the great preponderance of the alumina particles is taken to have a diameter of about 100 μm or less, then in general the slag retained is least for the conocyl motor and greatest for the long motor. About three horizontal test firings of a motor roughly similar to the short motor and about three horizontal firings and two vertical firings of a motor roughly similar to

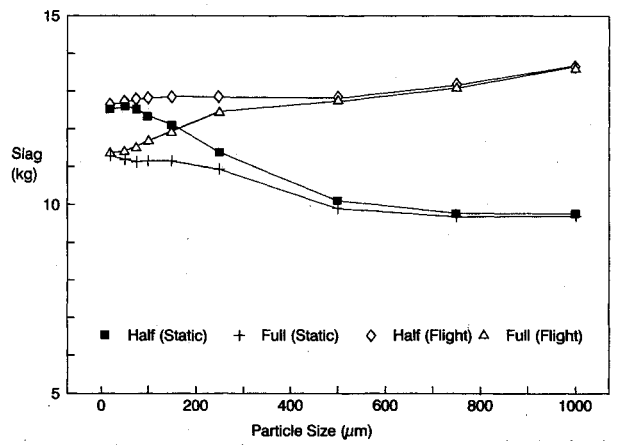

Fig. 13 Slag retained in the short motor as a function of particle diameter, for both static and flight conditions. The half-annulus and full-annulus models for the recirculation zone are examined. Here, $Y_{Al} = 0.16$ and $\rho_{sg} = 1850$ kg/m^3 (nominal conditions).

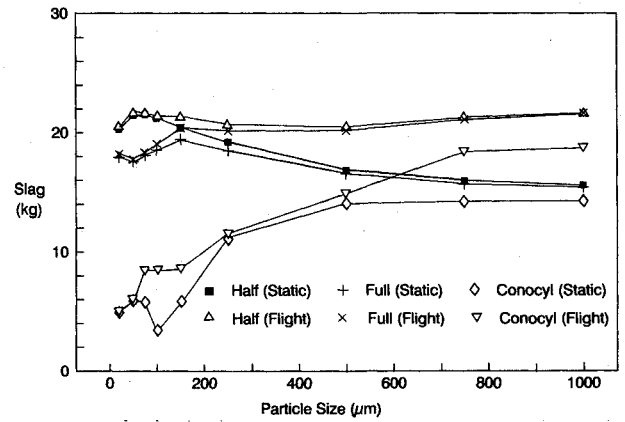

Fig. 14 Slag retained in the long and conocyl motors as a function of particle diameter, for both static and flight conditions. For the long motor, two recirculation-zone models are examined (see Figs. 5 and 13). The slag for each particle size is based on a distribution of alumina particles monodisperse at that size. Here, $Y_{Al} = 0.18$ and $\rho_{sg} = 1850$ kg/m^3 (off-nominal conditions).

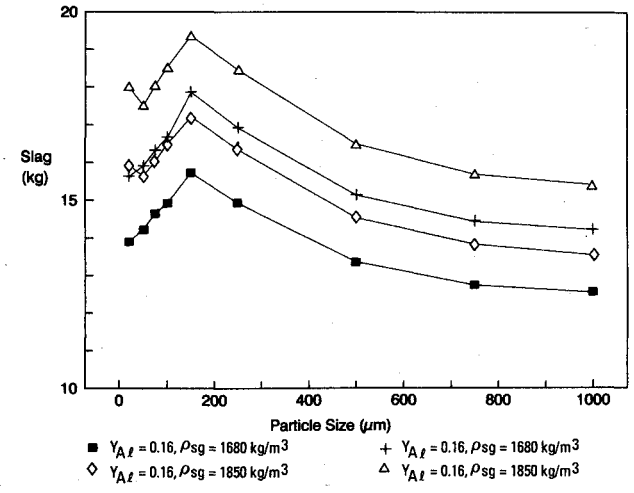

Fig. 15 Slag retained in the statically fired long motor with a full recirculation zone, as a function of alumina-particle diameter, for several values of the mass fraction Y_{Al} of aluminum in the grain and of the total density ρ_{sg} of the metallized grain.

the long motor have been carried out over the past six years; the horizontal firings were conducted near Brigham City, Utah, and the vertical firings at China Lake, California.[13] The slag retentions for nominally identical cases varied by about 15%. Typical slag retention for the short motor was about 18 kg and for the long motor about 50 kg. The values computed here hover around 12 kg for the short motor and 20 kg for the long motor. Reasons for the discrepancy include differences in grain and casing geometries and approximations in the analysis (especially in estimation of the recirculatory flow and in the decoupling of the gas and solid phases).

Since $\rho_{sg} = \rho_1 + \rho_2$, where ρ_2 is the mass of grain that evolves to alumina per volume of grain, and since forming each unit mass of alumina from the grain requires 1.89 times the mass of aluminum in the alumina, then

$$\rho_{sg} = \rho_1 + 1.89\ Y_{Al}\ \rho_{sg}, \quad \text{so} \quad \rho_1 = \rho_{sg}(1 - 1.89\ Y_{Al}) \qquad (9)$$

Thus, the effect of modest changes in the aluminum mass fraction on particle paths (and hence on the slag collected) may be roughly estimated. The calculation is limited to small changes in aluminum content since we hold all other parameters fixed (including p_0, T_0, $\dot{R}_s$, etc). Figure 15 presents results for the slag retention by the long motor under static firing with a full exit-plane-annulus recirculation zone, for several variations from nominal values of the grain density ρ_{sg} and the aluminum mass fraction Y_{Al}. Since the gas-phase flowfield is altered (because the gas flux at the gas-grain interface is altered) by these variations in the grain properties, there is a modest departure from simple linearity in the slag accumulation as a function of aluminum content of the grain, at least for some alumina-particle sizes.

Concluding Remarks

The presence of grain at the aft end of the motor during most of the burn precludes the existence of a holding volume in which slag may accumulate. Furthermore, the presence of a grain tends to result in a radially inward flux of gas evolving from the grain, so that the molten alumina particles are convected toward the mouth of the nozzle. For equalization of the gas/grain-interface area during the duration of the burn and to achieve a temporally constant mass throughput, slots in the grain may be needed; however, such slots seem better sited near the nose end, rather than the aft end, of the motor. Particles from the nose end of the grain tend to enter the nozzle nearer to the axis of symmetry, and a reduced radially inward velocity component near the nose end poses less slag-retention complication.

The last-to-burn portion of the grain toward the aft end of the motor in particular seems to be a likely contributor to the retained slag, since the alumina particles generated from this portion of the grain are injected far from the axis of symmetry and near to any recirculatory flow. Thus one might consider reducing the aluminum content of this portion of the grain. Such nonhomogeneity in aluminum content might not be prohibitively difficult to accomplish were current grain-casting procedures altered. Such a reduction in aluminum content does compromise performance but may obviate such problems as slug-type, asymmetric expulsion of accumulated slag, and slag interference with nozzle vectoring.

Another slag-reducing procedure might be to forgo recession of the nozzle; though such a design might helpfully alter the recirculatory-flow domain, such a design also increases the motor length and may exacerbate interference by slag with the thrust-vector-control mechanism.

With respect to further analysis, two self-consistency checks on the analysis may be undertaken. First, except for very shortly after ignition, the throat of the sonic nozzle must have a throughput consistent with the burn rate of the grain. This requirement places a constraint on the motor chamber pressure. Furthermore, that pressure might not be justifiably approximated as spatially homogeneous: a significant finite axial pressure gradient may be associated with the acceleration of the alumina particles. Finally, other parametric investigations (e.g., of a grain configuration with a long tapered bore) remain to be explored, although the methodology for treating a tapered bore has been given (see the Appendix of Ref. 4).

Acknowledgments

This work was performed under contract F04704-89-C-0037 with the U.S. Air Force Ballistic Missiles Office, San Bernardino, California. The authors are very grateful for many helpful discussions with George Carrier of Harvard University and James Kliegel of TRW Space and Technology Group.

References

[1]Price, E. W., "Combustion of Metallized Propellants," *Fundamentals of Solid-Propellant Combustion,* Vol. 90, Progress in Astronautics and Aeronautics, AIAA, New York, 1984, pp. 479–513.

[2]Rudinger, G., *Fundamentals of Gas-Particle Flow,* Elsevier, Amsterdam, The Netherlands, 1980, pp. 1–28.

[3]Bartley, C. E., and Mills, M. M., "Solid Propellant Rockets," *Jet Propulsion Engines, High Speed Aerodynamics and Jet Propulsion,* Vol. 12, Princeton Univ., Princeton, NJ, 1959, pp. 521–624.

[4]Carrier, G., Fendell, F., Brent, D., Kimbrough, C., Loucks, S., Hess, E., and Acosta, P., "Simple Modeling of Particle Trajectories in Solid-Rocket Motors," *Journal of Propulsion and Power,* Vol. 7, No. 2, 1991, pp. 185–195.

[5]Ma, Y.-C., Fendell, F., Brent, D., and Kliegel, J., "The Constant-Fractional-Lag Model for Axisymmetric Two-Phase Flow," *Journal of Propulsion and Power,* Vol. 7, No. 5, 1991, pp. 700–707.

[6]Culick, F. E. C., "Rotational Axisymmetric Mean Flow and Damping of Acoustic Waves in a Solid Rocket Propellant," *AIAA Journal,* Vol. 4, No. 8, 1966, pp. 1462–1464.

[7]Haloulakos, V. E., "Slag Mass Accumulation in Spinning Solid Rocket Motors," *Journal of Propulsion and Power,* Vol. 7, No. 1, 1991, pp. 14–21.

[8]Waesche, R. H. W., Sargent, W. H., and Marchman, J. F., III, "Space Shuttle Solid Rocket Motor Aft-End Internal Flows," *Journal of Propulsion and Power,* Vol. 5, No. 6, 1989, pp. 650-656.

[9]Borass, S., "Modeling Slag Deposition in the Space Shuttle Solid Rocket Motor," *Journal of Spacecraft and Rockets,* Vol. 21, No. 1, 1984, pp. 47–54.

[10]Kliegel, J. R., "Gas-Particle Nozzle Flow," *Ninth Symposium (International) on Combustion,* Academic, New York, 1963, pp. 811–826.

[11]Chang, I.-S., "One and Two-Phase Nozzle Flows," *AIAA Journal,* Vol. 18, No. 12, 1980, pp. 1455–1461.

[12]Batchelor, G. K., *An Introduction to Fluid Mechanics,* Cambridge Univ. Press, Cambridge, England, UK, 1967, pp. 536–538.

[13]Brent, D., private communication, TRW Space and Technology Group, Redondo Beach, CA 1991.

James A. Martin
Associate Editor